POSTPRINT version

Published in: Ceramics International ***44*** *(2018) 14865–14872* https://doi.org/10.1016/j.ceramint.2018.05.120

Continuous processing of $Bi_2Sr_2CaCu_2O_{8+\delta}$ precursor powders

C. Laliena[1], H. Amaveda[1], B. Özçelik[2], E. Martínez[1], G. F. de la Fuente[1], L. A. Angurel[1]*

[1]ICMA (CSIC-University of Zaragoza), María de Luna, 3, E50018 Zaragoza (Spain)

[2]Cukurova University, Adana (Turkey)

ABSTRACT

A continuous solid-state process inside a roller furnace has been used to fabricate Bi-2212 powders. These powders were synthesized for their use as precursors to obtain textured monoliths by laser induced directional solidification. A thermal cycle has been defined, which depends on the length of the furnace, the prefixed temperature profile and the velocity of the sample inside the furnace. Powder properties have been studied as a function of the number of processing cycles. Phase evolution has been analyzed using X-ray diffraction, while other relevant properties of the powders, including grain size distribution, thermal behavior and temperature dependence of the AC susceptibility, have also been measured. These properties have been compared with those of commercial powders and precursors prepared using a standard solid-state protocol. Textured samples using these continuous solid-state precursors exhibit superconducting properties comparable to those similarly processed but prepared from commercial powders.

Keywords: Superconductor; Bi-2212; Continuous processing

1.- Introduction

Within the Bi-Sr-Ca-Cu-O (BSCCO) family of superconductors [1,2], $Bi_2Sr_2CaCu_2O_{8+\delta}$ (Bi-2212) and $Bi_2Sr_2Ca_2Cu_3O_{10+\delta}$ (Bi-2223) with critical temperatures $T_c \approx 92$ K and 110 K, respectively, have been the most widely studied phases in the past decades due to their possible technological interest [3,4]. Despite its lower critical temperature, Bi-2212 phase presents certain advantages over Bi-2223 as it exhibits higher stability, allows simpler reaction conditions, and can be manufactured as round wires [5] instead of tapes, greatly preferred in magnet technology. However, its high superconducting anisotropy restricts applications to temperatures below ~ 10 K in case of strong magnetic fields (> 10 T), or to low magnetic fields at higher temperatures. This superconductor has been used to manufacture current leads [6], and it is receiving nowadays increasing attention for further developments of existing applications requiring very high-field magnets beyond the limits of the current Nb_3Sn technology, such as nuclear magnetic resonance (NMR) or particle accelerators [5].

In order to optimize the superconducting properties of the wires, tapes or bulk materials, their microstructure has to be controlled. In Bi-2212 materials, the required texture can be induced using melting techniques with a very controlled solidification process. In addition, this material exhibits incongruent melting. Different phases are thus present after solidification, essentially with stoichiometry close to $Bi_2Sr_2CuO_{6+\delta}$ (Bi-2201) and some Bi-free oxides. In consequence, a final heat treatment is required to form the superconducting Bi-2212 phase while maintaining the grain texture achieved during solidification [7, 8]. Obviously, the characteristics of the precursors play an important role in the final properties of the wires and bulk textured materials. Several studies have explored the influence of the precursor composition on the properties of the final textured material [9, 10]. It was observed that changes in the precursor stoichiometry modify the proportions of the different phases that are present after the melting process, and affect the microstructure and superconducting properties of the final processed material.

As previously reviewed by Angurel et al. [11, 12], among the texturing methods reported in the literature to produce bulk textured materials, Laser Floating Zone (LFZ) and Laser Zone Melting (LZM) processing methods are appropriate to obtain highly textured BSCCO superconductors with a Bi-2212 stoichiometry.

On the other hand, precursor Bi-2212 powders, which are commercially available, can also be produced at the laboratory scale. Different synthesis routes have already been proposed [13-16], and previous works have demonstrated a relatively low influence of the powder precursor synthesis method in subsequent LFZ and LZM processed materials [14-16]. Laser induced directional solidification processes produce phase segregation along the sample cross-section, with a highly textured granular microstructure in the regions close to its surface. The superconducting performance of these materials is mainly associated with the texture quality in this region. It has been observed that, when different powder synthesis methods are used, small changes in the microstructure of this external region barely affect the sample's superconducting properties.

Since the price of commercial Bi-2212 powders has been increasing within the last several years, reaching levels above 2 k€/kg, it seems appropriate to explore alternative Bi-2212 powder precursor synthesis routes, which may be industrially scalable and considerably cheaper than those presently available from commercial suppliers.

The most common methods to produce Bi-2212 powders follow conventional solid-state reaction processes, which, at the laboratory scale, are limited to small quantities of the order of 250-500 g. This is very low for an industrially scalable process because it requires processing the powder in

several batches, compromising thus its stoichiometry homogeneity and, in consequence, its use for further processing.

The aim of this work is to overcome the above-mentioned problems by developing a novel continuous powder processing method based on the use of a continuous furnace. This methodology, which is used routinely by the ceramic industry, can be applied to prepare Bi-2212 precursor powders for melt texture processes in shorter times, without limitation regarding production volume and uniformity. This paper describes a continuous solid-state processing method, as well as the characteristics of the obtained powders at several stages of this process. A comparison between these precursor powders with those fabricated with the standard solid-state process [14,15], as well as with commercially available powders, is also presented.

2.-Experimental

2.1. Powder preparation

Three different types of Bi-2212 powders have been compared in this study, including commercially available powders, as well as standard solid-state and continuous solid-state synthesized powders. Their synthesis is described as follows.

2.1.1. Commercial powders (C)

The analyzed commercial powders, named C, were provided by Nexans SuperConductors GmbH and had the following stoichiometry: $Bi_{2.18}Sr_{1.98}Ca_{0.87}Cu_{1.97}O_x$.

2.1.2. Standard solid-state powders (SSS)

Precursor powders, named SSS, were made from a mixture of raw oxides and carbonate starting materials with a Bi-Sr-Ca-Cu stoichiometry of 2.1:2:1:2, using the standard solid-state reaction method. The Bi-2212 powders were prepared from: Bi_2O_3 (99.9 % metal basis, Sigma Aldrich, mean particle size lower than 10 μm), $SrCO_3$ (99.9 % metal basis, Sigma Aldrich), $CaCO_3$ (99.5 % metal basis, Alfa Aesar) and CuO (99.7 % metal basis, Alfa Aesar, maximum particle size lower than 74 μm).

Initially, the precursor powders were dried at 350 ºC during 6 h. Subsequently, the required quantities of components (Table I) were mixed with 100 ml of heptane (C_7H_{16}) for 1 h at 300 rpm in a Retsch PM100 planetary ball mill. Typically, a quantity of $\sim$115 g of precursor mixture is required to obtain 100 g of $Bi_{2.1}Sr_2CaCu_2O_x$ (see Table I). The used mill has a sun disk of radius r_p = 7 cm. The milling was performed in an agate jar of inner radius r_v = 38 mm, with 50 agate balls of radius r_b = 5 mm and 1.4 g mass each. Thus, the agate ball-to-powder mass ratio, β, was always kept at $\sim$0.7. In this apparatus, the amount of milled powder for each run is limited to about 100 g. After having finished the milling process, the residual heptane was eliminated by slow drying at 120 ºC for 24 h in a stove.

Table I: Quantities of raw oxide and carbonate precursors used to obtain 100 g of Bi-2212 in the 2.1:2:1:2 proportions.

Precursor	*M* (g mol^{-1})	*n* (mol)	*W* (g)
Bi-2212	909.28	0.11	100
Bi_2O_3	456.96	1.05	53.81
$SrCO_3$	147.63	2.00	32.47
$CaCO_3$	100.09	1.00	11.01
CuO	79.55	2.00	17.50

The mixed and milled powder is thermally calcined in a muffle furnace, in air atmosphere, at 760 ºC for 16 h in order to partially decompose the alkaline earth carbonates. Two additional sintering processes at 830 ºC for 16 h were performed to form the Bi-2212 phase. After each heat treatment, it is essential to mill again the powder, in order to avoid the formation of hard and bulky aggregates.

Typically, the maximum amount of precursors that can be processed by this method at the same time is ~ 100 g, depending on the type of furnace used. This is limited by the maximum allowed temperature differences in the powder batch during heat treatment, associated to the inherent temperature gradients inside the muffle furnace. This fact constitutes the most restrictive point of the sintering process, since the maximum amount of powders that can be milled in each step can be increased with an adequate milling system.

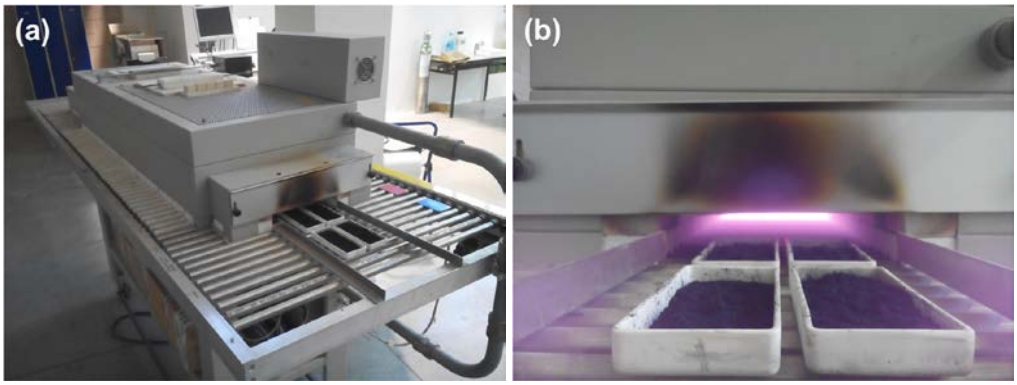

Figure 1: (a) Photograph of the 4-m long continuous furnace used for the CSS powder processing. (b) Photograph of the four ceramic sample holders that contain approximately 500 g of precursor powders entering the furnace. The pinkish intense light emitted from the furnace is originated from its red-hot resistances.

2.1.3. Continuous solid-state powders (CSS)

The continuous solid-state precursor powders, CSS, are produced from the same raw oxide and carbonate powder mixture as in the standard solid-state reaction, but using a new procedure described as follows.

In this process, the heat treatments in a muffle furnace have been substituted by a heat treatment in a continuous furnace, which allows processing much larger quantities of powders with reproducible properties. The 4 m long furnace used in this study is presented in Figure 1(a). It contains three zones with independent temperature control. This allows imposing a temperature profile inside the furnace with an initial preheating zone, a central sintering/annealing zone and a final cooling zone. Temperatures up to 1200 ºC can be reached inside the furnace. The movement of the sample inside the furnace is achieved by means of ceramic cylinders that rotate at a given velocity. Sample velocities from 0.5 m h^{-1} to 4 m h^{-1} can be programmed in this apparatus.

In this work, 500 g of oxide and carbonate precursors were processed at the same time in this continuous furnace (see Figure 1(b)) using four ceramic crucibles that contained ~ 125 g each. The temperatures of the preheating and cooling zones of the furnace were fixed at 650 ºC, and that of the sintering zone at 800 ºC. The crucible displacement was set at 1.5 m h^{-1}, thus making an approximate total thermal cycle of 2.5 h, with ~ 45 min soaking at the highest temperature zone. This continuous thermal cycle was repeated up to seven times for the raw precursor powder mixture subjected to study. In order to identify the powders, they have been named CSSX, where X is the number of thermal cycles followed by the powder.

To break the agglomerates produced during the heat treatment and to facilitate the chemical reaction on the subsequent thermal cycles, after each cycle, the precursor powder mixture from each ceramic crucible (~ 125 g) was individually ball milled for 15 min at 300 rpm with 80 ml of heptane, using the same jar and number of balls as for the standard solid state procedure. The residual heptane was then evaporated at 120 ºC during 24 h. This is particularly critical within the first two or three thermal cycles, when most agglomerates are formed.

2.2.- Characterization methods

The phase composition of different precursor powders was analyzed by means of XRD patterns, collected at room temperature on a RIGAKU D-max/2500 X-ray diffractometer using Cu Kα radiation. A semi-quantitative phase composition analysis was performed from these XRD patterns using the reference intensity ratio (RIR) of each phase. RIR is defined as I/I_{cor}, where I is the intensity of the 100% peak of the analysed phase, and I_{cor} is the intensity of the 100% peak of a reference phase, taken by convention to be α-Al_2O_3 (corundum) in a 50:50 mixture by weight.

The particle size distribution of the studied powders was analyzed using a Beckman Coulter LS 13 320 laser diffraction particle size analyzer. Grain morphology was studied by Scanning Electron Microscopy in a field-emission scanning electron microscope (FE-SEM, Carl Zeiss MERLIN) using a secondary-electron (SE) and an in-lens secondary electron detector.

In addition, thermogravimetric analysis (TGA) and differential scanning calorimetry (DSC) of the different powders were also performed using a SDT Q600 system that allows a simultaneous registry of weight loss (TGA) and heat flow changes (DSC) along programmed temperature scans. DSC was calibrated with a sapphire standard and samples of about 15 mg were laid onto the tarred alumina pans. Air was used as the purge gas at a flow rate of 100 ml min^{-1}. The precursor was heated at a rate of 10 ºC/min from RT up to $\sim$1000 ˚C. The enthalpy of fusion (in J/g) can be calculated by integration of the endothermic fusion peak.

Finally, the superconducting properties of the processed powders were analysed using a SQUID-based Quantum Design MPMS-5T system performing AC susceptibility measurements as a function of temperature, $\chi_{ac}(T)$, in zero DC magnetic field and AC fields with an amplitude of 0.1 mT and a frequency of 120 Hz.

3.- Results and Discussion

3.1. Evolution of the phase composition

The evolution of the phase composition during the different cycles of the continuous solid-state process has been monitored using XRD patterns. The obtained diffractograms are presented in Figure 2. The pattern at the top of the figure corresponds to the initial raw mixture of oxides and carbonates (powder CSS0), which shows the expected phases: Bi_2O_3, $SrCO_3$, $CaCO_3$ and CuO (see Table I). Below is the pattern of the precursor powders after the first thermal treatment in the continuous furnace (powder CSS1). The strongest peaks associated with Bi_2O_3 (see for instance the peaks between 2θ=26º and 28º) are no longer present, and also the $CaCO_3$ phase cannot be detected. The presence of the characteristic peak at 7.2º indicates that the Bi-2201 phase has started to form in this first stage. Other Bi-containing compounds also appear to be present, identified by Naumov et al in [17] by the general formula $Bi_4(Ca_{2-x}Sr_{1.5-x})O_{9.5}$. These exhibit a wide composition range and are difficult to identify by XRD. The presence of $SrCO_3$ and CuO in trace amounts is confirmed, while it is important to point out that the Bi-2212 phase is not detected in these CSS1 powders.

The diffraction pattern that corresponds to the precursor powders after the third thermal treatment (CSS3) shows that the Bi-2212 phase began to form; a remarkable fact, considering the low number of heat treatments imposed. Note that, in addition to the Bi-2201 phase, there are some low intensity peaks of $SrCO_3$, CuO and Bi-containing compounds, indicating that some small amounts of these phases are still present in these powders.

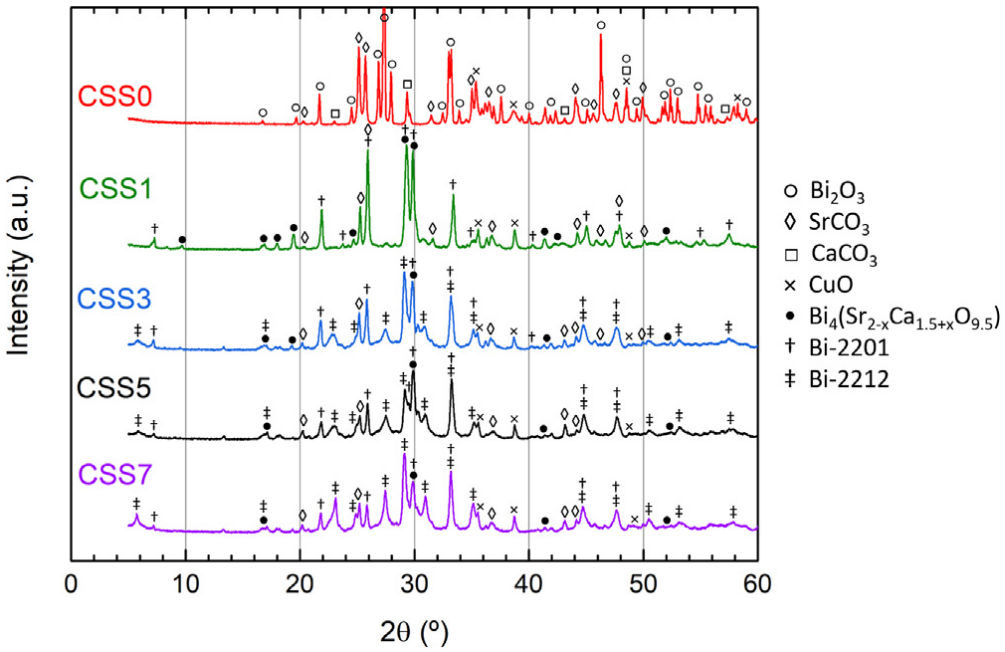

Figure 2: XRD patterns of the powders at different stages from the raw initial mixture (CSS0) to the final powders after seven heat treatments (CSS7). Identified phases are shown with the symbols indicated in the right.

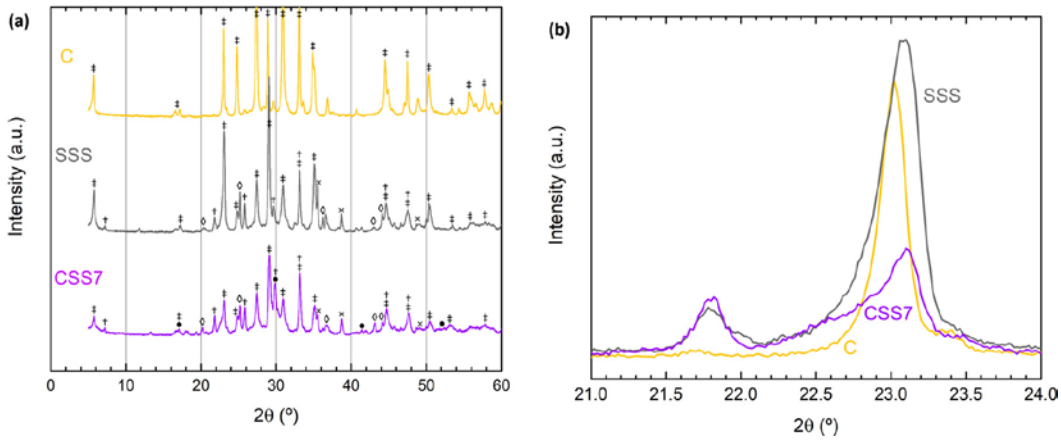

Figure 3: (a) XRD patterns of the C, SSS and CSS7 precursor powders. The different phases are identified by the same symbols as in Fig. 2. (b) Detail of Bi-2212 phase (008) peak (2θ = 23.1º) showing broadening and a small shift.

The XRD pattern after the fifth heat treatment in the continuous furnace (CSS5) suggests the presence of Bi-2212 and Bi-2201 as major phases. The relative evolution of these two phases has been analyzed by the ratio of the intensities of the 2θ = 23.1º (Bi-2212) and the 2θ = 21.8º peak (Bi-2201). This ratio was 0 in the case of the sample CSS1, 0.51 in CSS3 and 0.76 in CSS5. The peak intensities of the $SrCO_3$ and CuO phases are very similar in these three powders, which could indicate that the changes in the amount of these two phases are very small during the progressive continuous thermal processing steps.

It is worth noting that the pattern of the final precursor powders subjected to seven heat treatments (CSS7) does not show any significant differences with CSS5, except for the fact that the intensity of the Bi-2212 peaks of CSS7 is slightly enhanced ($I_{23.1}/I_{21.8}$ = 1.85), meaning this transformation has evolved during this step. Table II collects the main phases and the composition (wt%) of the CSS7 and the SSS

precursor powders. This composition analysis was performed using the RIR of each phase. It is important to take into account that these Bi-based superconductors form by intercalation of the different phase layers. In consequence, the Bi-2212 phase, for instance, shows a broad range of compositions. For this reason, the values presented in Table II can be considered only as semi-quantitative estimates.

As mentioned above, Bi-2212 phase begins to form in the continuous solid-state process during the second or third heat treatment, reaching ~ 34 wt.% in the CSS7 sample. It must be noted that the sum of Bi-2201 and Bi-2212 phases reaches ~ 75 wt.%. The other 25 wt.% corresponds mainly to $SrCO_3$ and CuO. In the standard solid-state powders, the proportion of Bi-2212 phase is about 42 wt.%, but the sum of Bi-2201 and Bi-2212 phases is slightly lower than in the case of the continuous process (~ 62 wt.%).

In Figure 3 the XRD patterns of the C, SSS and CSS7 precursor powders are compared. Bi-2212 phase peaks are thus observed sharper for the C powder than for SSS and CSS7 powders in this Figure. When comparing SSS and CSS7 powders, Bi-2212 peaks appear sharper and more prominent than those of the Bi-2201 phase ($I_{23.1}/I_{21.8} = 6.44$) in the SSS precursor, in good agreement with the results shown in Table II. Figure 3(b) shows a detail of these XRD patterns around the (008) peak of the Bi-2212 ($2\theta = 23.1^o$). Besides a small shift in the position ($2\theta = 23.0^o$ in C and $2\theta = 23.1^o$ in SSS and CSS7 powders), the peaks of both solid-state powders are broader than that of the C powder. This can be explained by the presence of intergrowths of Bi-2201 in the Bi-2212 grains [9] during the solid state reaction process, which also complicates the phase quantification by XRD, as previously mentioned.

Table II: Phase composition (wt %) of the CSS7 and SSS precursor powders obtained with a semi-quantitative analysis using the RIR of each phase.

Precursor Powders	Bi-2201	Bi-2212	$SrCO_3$	CuO
CSS7	41.2	33.6	14.1	11.1
SSS	19.9	42.0	21.0	17.1

Table III: Particle size distribution parameters d_{10}, d_{50} and d_{90} for some precursor powders.

Precursor Powders	d_{10} (µm)	d_{50} (µm)	d_{90} (µm)
C	0.10	1.18	2.18
SSS	4.74	22.95	55.59
CSS5	4.19	15.81	41.70
CSS7	4.05	16.84	42.45

3.2. Particle size distribution

Figure 4 shows a comparison of the measured particle size distribution of the SSS, CSS5 and CSS7 precursor powders. The parameters d_{10}, d_{50} and d_{90}, characterising the powder particle size distribution, are collected in Table III for these powders, together with those corresponding to the commercial powder, which were provided by the manufacturer. The commercial powders present the smallest grain size by more than an order of magnitude. The three analyzed precursor powders prepared in this work, present very similar values of grain size, with no significant difference in the obtained values among the continuous solid-state precursor powders after five and seven heat treatments. This is expected because the powders are ball milled after every heat treatment in the continuous furnace, thus homogenizing the different phases present and their particle size distribution. The main differences between both powders are observed in the region between 30 µm to 50 µm, where the number of

particles is higher in the powders that have been processed seven times. When we compare these distributions with that of the SSS powders, we observe that the grain size distribution of SSS is similar, although slightly shifted to higher values. This difference is probably due to the larger number of milling cycles performed on the CSSX precursor. Curves presented in Figure 4 also show that the volume percentage of particles with sizes between 0.4 μm and 2 μm is very similar in all three powders.

All these results have also been confirmed by FE-SEM observations of the different powders, as presented in Figure 5. Clearly, the differences in size of one order of magnitude can be observed if the image of powder C (Figure 5(a)) is compared with the images taken in the other three powders. Figure 6 shows the C and CSS7 powders using a higher magnification for more detail. Note that these images were taken using the in-lens detector, which is a high efficiency annular secondary electron detector used to map the surface structure of a sample. These images clearly show that the grains are agglomerates of stacked platelets.

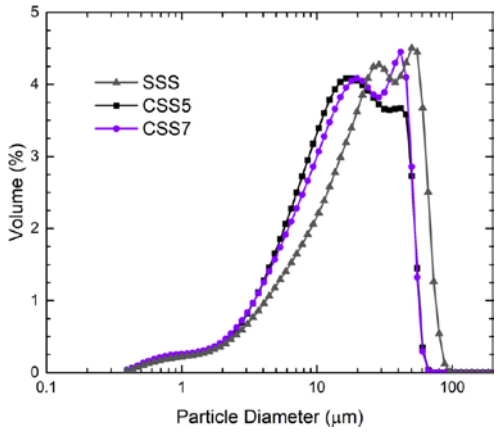

Figure 4: Particle size distribution of the SSS, CSS5 and CSS7 precursor powders.

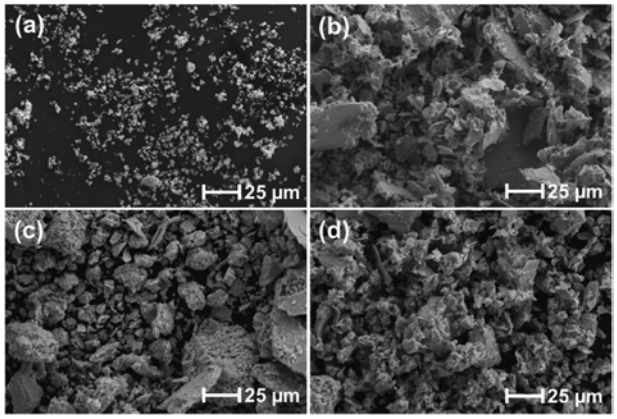

Figure 5: FE-SEM images of the different analyzed powders using a secondary-electron (SE) detector: (a) C, (b) SSS, (c) CSS5, and (d) CSS7.

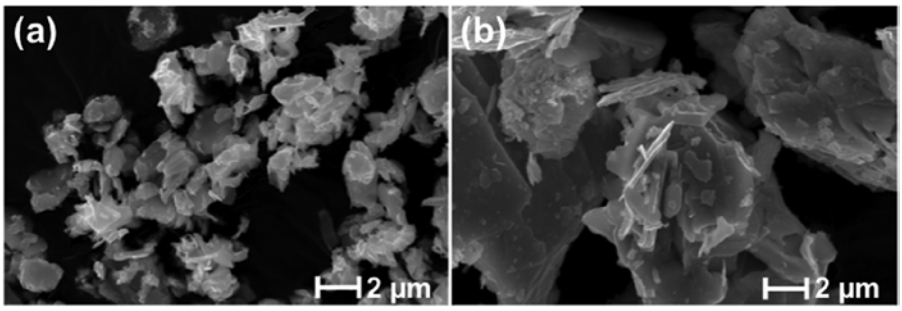

Figure 6: Detail of superconducting grains using an in-lens secondary electron detector for samples (a) C and (b) CSS7 using higher magnification than in Figure 5.

3.3. Melting behavior of the analyzed powders

As these powders are intended for use as precursors for a melt-texture process, it is important to study if the above-mentioned differences have any influence on their melting behavior. This has been analyzed by measuring the DSC-TGA curves.

The percentage of weight loss as a function of temperature is displayed in Figure 7 for different precursor powders. The commercial powders present a weight loss of about 2 % between 100 and 250 ^{o}C, which can be due to elimination of some hydroxide compounds that can be fixed in the surface of these small powders. This was expected since these powders have been stored for more that two years,

they are very fine and, consequently, they are more reactive in ambient air in comparison with the other powders subjected to this study.

Concerning the continuous solid-state precursors, CSS0 presents the greater weight loss as expected: up to 14 % at 1000 ºC. This is because the oxides and carbonates react to form the superconducting phase previously losing the carbon content in the form of CO and CO_2. In fact, as detailed in Table I, 114.8 g of oxides and carbonates are required to obtain 100 g of Bi-2212, which is in good agreement with the TGA measurement. It is observed that all these reactions start at temperatures bellow 600 ºC. CSS5, CSS7 and SSS precursor present very similar curves, so that the formation of the Bi-2212 would be similar in all three cases. The slight difference between the weight loss of CSS5 and CSS7 powders (5 % and 5.5 %, respectively) indicates that additional heat treatments would not essentially change the precursor powder behavior. Comparing the curves of the SSS, CSS5 and CSS7 with the curve of sample C, it is observed that the small mass loss at high temperatures in samples C starts at approximately 650 ºC while, in the other three samples, it starts in the proximity of 750 ºC.

Figure 8 shows the temperature dependence of the heat flow required to keep constant the heating ramp. The temperature region where the fusion phenomena take place is shown in more detail in the inset. Mayoral *et al.* [18] showed that when low heating rates are used it is possible to distinguish the melting of different phases. They found that a small part of the sample melts at temperatures between 865 and 870 ºC, another fraction, associated with the Bi-2201 phase melts between 875 and 885 ºC, and the greater portion melts between 885 and 895 ºC. Data presented in the inset of Figure 7 shows that in the SSS, CSS5 and CSS7 precursors, a similar behavior is observed, with different melting phenomena above 870 ºC. The melting peaks of these powders are broader towards lower temperatures, which is expected due to the variations in the stoichiometry and to the presence of the lower melting temperature Bi-2201 phase [19] in these powders. The values at which the main melting peak occurs and the values of the energy involved in the endothermic peak are collected in Table IV. In the case of sample C, as the main phase is Bi-2212, only one peak is observed. In contrast, the CSS0 sample shows a different behavior showing an exothermic peak at 650 ºC, and a small step in the heat flow at 857 ºC showing that the Bi-2201 phase is forming. At temperatures above 890 ºC it is possible to detect the formation and melting of the Bi-2212 phase.

Mayoral *et al.* [18] also showed that the Bi/(Sr+Ca) ratio can modify the melting temperature up to 7 ºC, but without a clear trend when this ratio is changed. In addition, depending on this ratio the mechanism that controls the involved solid-state reactions are different. In this work, the used stoichiometries give a value of Bi/(Sr+Ca)=0.76 for the C powder and 0.7 for the other powders and they are considered as Bi-rich precursors. In the case of the solid-state precursor powders, where a multiphase is obtained, the mobility of reactants is accelerated by the formation of a liquid phase.

These results show a similar melting behavior of SSS, CSS5 and CSS7 powders. Taking into account powder properties and processing method requirements, we may conclude that CSS5 presents satisfactory characteristics to be used as precursor for melt-processed Bi-2212 materials, for example, in laser texturing [11, 12]. Additional heat treatments do not produce substantial differences in the melting process of these powders.

Table IV: Melting temperatures and enthalpy changes of the Bi-2212 phase for the different precursor powders.

Precursor Powders	T (ºC)	ΔH (J/g)
C	887.88	82.6
SSS	891.11	102.9
CSS0	887.18	35.8
CSS5	885.27	87.9
CSS7	888.53	113.0

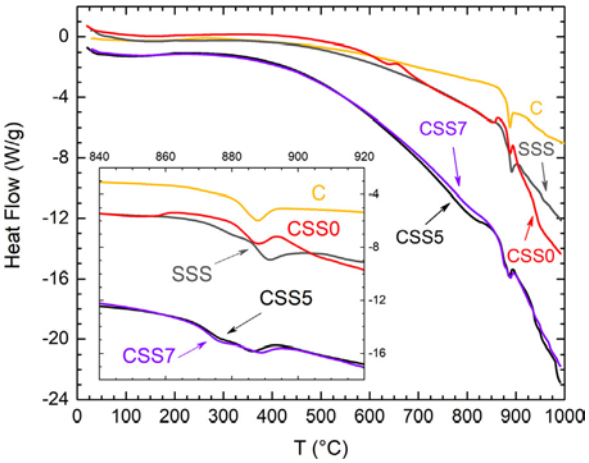

Figure 7: TGA of the C, SSS, CSS0, CSS5 and CSS7 precursor powders.

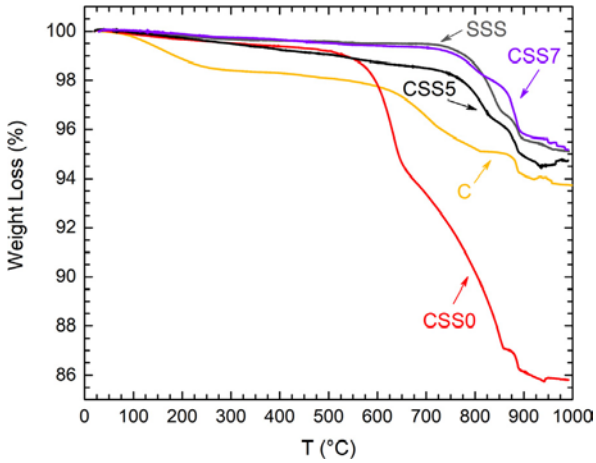

Figure 8: DSC of the C, SSS, CSS0, CSS5 and CSS7 precursor powders.

3.4. Superconducting properties of precursor powders.

Figure 9(a) displays the in-phase component of the AC susceptibility, χ', as a function of the temperature for C, SSS, CSS5 and CSS7 powders. The same data together with the out-of-phase component, both scaled by $|\chi'(5\ K)|$, are also shown in (b) and (c). It is observed that all these samples show superconducting behaviour, but with remarkably smaller χ' values in the case of commercial powders, by approximately one order of magnitude at low temperatures. This behaviour can be qualitatively explained by the differences in the grain sizes between these powders (Table III and Figure 5) and taking into account the value of the in-plane London penetration depth in this material, $\lambda_{ab}(0)$, which is ~ 0.25 μm [20], the same order of magnitude as the grain size.

As discussed by Campbell *et al* [21], this is an important point to consider when AC susceptibility measurements are analysed. Clem and Kogan [22] presented the calculation of the magnetic moment, μ, of a superconducting spherical particle (radius R) as a function of the ratio $x=R/\lambda$ when a weak magnetic field (H) is applied:

$$\mu = -(H R^3/2)P(x)$$

where λ is the average London penetration depth and $P(x) = 1 - (3/x)\coth(x) + 3/x^2$.

Although the Bi-2212 grains have a platelet-like shape, they are arranged in the form of agglomerates with rather spherical configuration, as can be seen in Figure 6. P(x) is proportional to the percentage of the sample volume that would contribute to the diamagnetic signal. Table V shows the values of P(x) at low temperatures when $2R = d_{50}$ and d_{90} of each powder is considered. Figure 9(a) shows that the diamagnetic signal of powder C is approximately the 12% of the diamagnetism of the SSS powder. This can be explained taking into account that the contribution of smaller grains in powder C has a negligible effect on the diamagnetic signal and, that the grains associated to the bigger sizes are able to shield only a 22% of the volume.

The differences in the temperature dependence presented in Figures 9 (b) and (c) can also be explained considering the temperature dependence of the London penetration depth [22]. Transitions become broader as the particle size is reduced [21], following the trends presented in Figure 9(b).

In consequence, with these results, it is considered that after five heat treatment cycles in a continuous furnace, the quality of the precursor powders obtained is sufficient to fabricate satisfactory high critical

temperature Bi-2212 superconductor ceramic monoliths by Laser Zone Melting (LZM). In order to confirm these ideas, these powders have been used to fabricate LZM textured samples and it has been observed that the molten volumes have an uniform microstructure and the transport critical current values measured on representative samples at 77 K, based on these powders, are approximately at 75% of the values obtained on samples fabricated using the commercial powders under the same texturing parameters.

Table V: Evolution of P(R/λ (0)) for some characteristic grain sizes in the different powders

Precursor Powders	d_{50} (μm)	P(R/λ (0))	d_{90} (μm)	P(R/λ (0))
C	1.18	0.08	2.18	0.22
SSS	22.95	0.87	55.59	0.95
CSS5	15.81	0.82	41.70	0.93
CSS7	16.84	0.83	42.45	0.93

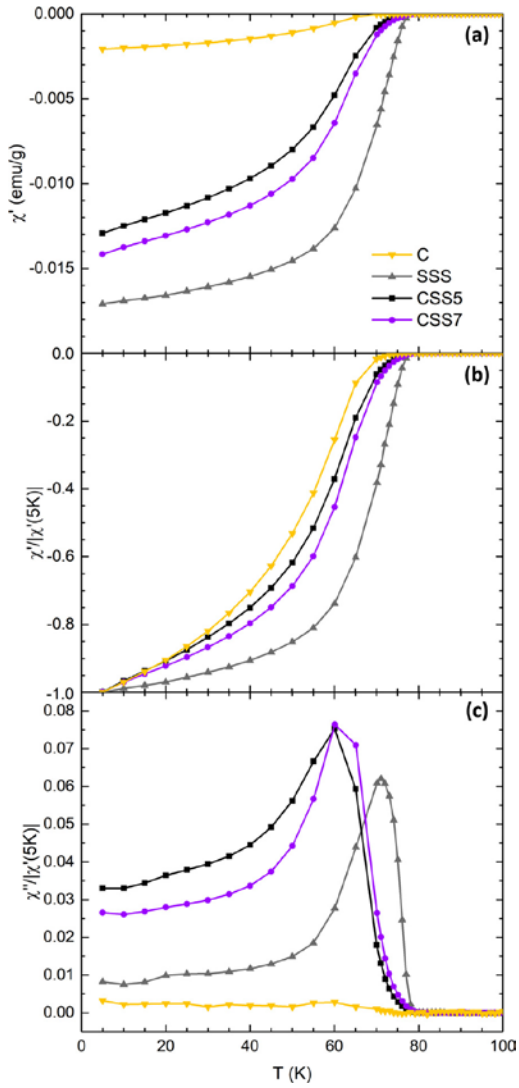

Figure 9. (a) Temperature dependence of the in-phase component of the AC susceptibility, χ´, for C, SSS, CSS5, CSS7 precursors. Values of the (b) in-phase and (c) out-of-phase components scaled to |χ´(5 K)|. The same symbols are used in the three figures.

4.- Conclusions

The results presented in this work show that it is possible to obtain Bi-2212 powders from oxide and carbonate raw precursors using a continuous solid-state fabrication process. The use of a 4-m long continuous furnace allows controlling the sample velocity and provides three zones where the temperature can be controlled independently, thus enabling prefixed temperature profiles and heat treatment durations. With this equipment, the Bi-2212 phase begins to form after three thermal cycles and provides it in sufficient content for melt processing after five cycles. Additional treatments facilitate further transformation of Bi-2201 into Bi-2212, but do not induce significant changes in the overall properties of the powders, such as superconducting properties and melting behavior. The behavior of these CSS powders exhibit similar properties than those obtained using a SSS process. In comparison with the commercial powders, the size of the CSS powders are one order of magnitude higher and the amount of Bi-2201 and other phases are relevant but during laser melting techniques, it is possible to obtain a uniform melting. In consequence, after five processing cycles, these powders have reached the required performance to be used as precursors in the processing of textured Bi-2212 materials using melting techniques and providing, thus, increased efficiency and significantly lower processing costs than equivalent, conventional methods. Textured samples fabricated with these powders have reached critical current values of the same order of magnitude than those obtained using commercially available powders.

Acknowledgements

This work was supported by the Spanish Ministerio de Economía y Competitividad and the European FEDER Program (project ENE2014-52105-R), and by the Gobierno de Aragón (research groups T12, T87 and T54_17R). The authors acknowledge the use of Servicio General de Apoyo a la Investigación-SAI, University of Zaragoza.

References

[1] C.Michel, M.Hervieu, M.M.Borel, A. Gran din, F.Desland, J. Provost, B.Raveau, *Superconductivity in the Bi-Sr-Cu-O system* Z Phys B **68** (1987) 421; doi.org/10.1007/BF01471071

[2] P. Majewski, *BiSrCaCuO High-T_c Superconductors*, Adv Mater **6** (1994) 460-469; doi.org/10.1002/adma.19940060604

[3] H.G. von Schnering, L. Walz, M. Schwarz, W. Becker, M. Hartweg, T. Popp, B. Hettich, P. Müller, G. Kämpf, *The Crystal Structures of the Superconducting Oxides $Bi_2(Sr_{1-x}Ca_x)_2CuO_{8-\delta}$ and $Bi_2(Sr_{1-y}Ca_y)_3Cu_2O_{10-\delta}$ with $0 \leq x \leq 0.3$ and $0.16 \leq y \leq 0.33$,* Angew Chem Int Ed Engl **27** (1988) 574-576; doi.org/10.1002/anie.198805741

[4] F. Kametani, J. Jiang, M. Matras, D. Abraimov, E.E. Hellstrom, D.C. Larbalestier, *Comparison of growth texture in round Bi2212 and flat Bi2223 wires and its relation to high critical current density development*, Scientific Reports **5** (2015) 8285; doi.org/10.1038/srep08285

[5] D.C. Larbalestier, J. Jiang, U.P. Trociewitz, F. Kametani, C. Scheuerlein, M. Dalban-Canassy, M. Matras, P. Chen. N.C. Craig, P.J. Lee, E.E. Hellstrom, *Isotropic round-wire multifilament cuprate superconductor for generation of magnetic fields above 30T*, Nature Materials **13** (2014) 375-381; doi.org/10.1038/nmat3887

[6] L. García-Tabarés, J. Calero, P. Abramián, F. Toral, L.A. Angurel, J.C. Díez, R. Burriel, E. Natividad, R. Iturbe, J. Etxeandía, *Design, Fabrication and Tests of a 600 A HT_c current lead for the LHC Correction Magnets*, IEEE Trans Appl Supercond **11** (2001) 2543-2546; doi.org/10.1109/77.920386

[7] I. Pallecchi, A. Leveratto, V. Braccini, V. Zunino, A. Malagoli, *Investigation of inter-grain current density in $Bi_2Sr_2CaCu_2O_{8+\delta}$ superconducting wires and its relationship with the heat treatment protocol*, Supercond Sci Technol **30** (2017) 095005, doi.org/10.1088/1361-6668/aa77e6

[8] E. Natividad, J.C. Díez, L.A. Angurel, J.M. Andrés, *Successful Application of Simplex Methods to the Optimization of Textured Superconducting Ceramics*, J. Am. Ceram. Soc. **87** (2004) 1216-1221; doi.org/10.1111/j.1151-2916.2004.tb07715.x

[9] P. Li, G. Naderi, J. Schwartz, T. Shen, *On the role of precursor powder composition in controlling microstructure, flux pinning, and the critical current density of Ag/ conductors*, Supercond Sci Technol **30** (2017) 035004; doi.org/10.1088/1361-6668/30/3/035004

[10] E. Natividad, J. C. Díez, L.A. Angurel, J. M. Andrés, A.C. Ferrando, M.C. Mayoral, *Radial changes in the microstructure of LFZ-textured Bi-2212 thin rods induced by stoichiometry modifications*, Physica C **383** (2003) 379-387; doi.org/10.1016/S0921-4534(02)01459-4

[11] L.A.Angurel, G.F. de la Fuente, A.Badía, A.Larrea, J.C. Diez, J.I. Peña, E. Martínez, R. Navarro, *Textured BSCCO Superconductors Obtained via Laser Induced Directional Solidification* in Vol. 21, pp 1-31, *Studies of High Temperature Superconductors*, A.V. Narlikar, ed. World Scientific (1997).

[12] L. A. Angurel, J. C. Diez, G. F. de la Fuente, *Laser Induced Cylindrical Zone Melting of $Bi_2Sr_2CaCu_2O_{8+\delta}$ Superconductors*, Z. Anorg. Allg. Chem. **635** (2009) 1767-1772; doi.org/10.1002/zaac.200900267

[13] A. Sotelo, H. Szillat, P. Majewski, F. Aldinger, *Rapid synthesis of the Bi-2212 phase by a polymer matrix method*, Supercond Sci Technol **10** (1997) 717-720; doi.org/10.1088/0953-2048/10/9/013

[14] Miao, H., Díez, J. C., Angurel, L. A., de la Fuente, G. F., *Precursor powder influence on melt processing of high critical current BSCCO rods*, Supercond. Sci. Technol. **13** (2000) 1135; doi.org/10.1088/0953-2048/13/8/304

[15] A. Sotelo, Sh. Rasekh, M.A. Madre, J.C. Díez, *Precursor influence on the electrical properties of textured Bi-2212 superconductors*, J. Supercond. Nov. Magn. **24** (2011) 19-25; doi.org/10.1007/s10948-010-0894-6

[16] M.F. Carrasco, F.M. Costa, R.F. Silva, F. Gimeno, A. Sotelo, M. Mora, J.C. Díez, L.A. Angurel, *Textured Bi–Sr–Ca–Cu–O rods processed by laser floating zone from solid state or melted precursors*, Physica C **415** (2004) 163-171; doi.org/10.1016/j.physc.2004.08.010

[17] D.Yu. Naumov, L.P. Kozeeva, M.Yu. Kameneva, N.V. Kuratieva, N.V. Podberezskaya, *Structure and refinement of the composition of Bi-Sr-Ca-Cu oxide crystals*, Crystallography Reports **53** (2008) 216-222; doi.org/10.1134/S1063774508020089

[18] M.C. Mayoral, J.M. Andrés, M.T. Bona, L.A. Angurel, E. Natividad, *Approximation to the laser floating zone preparation of high temperature BSCCO superconductors by DSC*, Thermochim. Acta **409** (2004) 157-164; doi.org/10.1016/S0040-6031(03)00354-X

[19] A. Maljuk, C. Li, *Bi-Based High-T_c Superconductors*, in *Growth and Characterization of Bulk Superconductor Material*, Ed by D. Chen, C. Lin, A. Maljuk and F. Zhou, Springer International Publishing, Switzerland (2016), 47-114.

[20] T. Shibauchi, A. Maeda, H. Kitano, T. Honda, K. Uchinokura, *Microwave complex conductivity in single crystals of $YBa_2Cu_3O_7$ and $Bi_2Sr_2CaCu_2O_y$, Physica C* **203** (1992) 315-319; doi.org/10.1016/0921-4534(92)90038-E

[21] A.M. Campbell, F.J. Blunt, J.D. Johnson, P.A. Freeman, *Quantitative determination of percentage superconductor in a new compound*, Cryogenics **31** (1991) 732-737; doi.org/10.1016/0011-2275(91)90236-P

[22] J.R. Clem, V.G. Kogan, *Theory of Magnetization of Granular Superconductors: Application to High-T_c Superconductors*, Jpn. J. Appl. Phys 26 (1987) 1161-1162; doi.org/10.7567/JJAPS.26S3.1161